Int. J. Electrochem. Sci., 16 **(2021)** Article ID: 210323, doi: 10.20964/2021.03.46

International Journal of
ELECTROCHEMICAL
SCIENCE
www.electrochemsci.org

Short Communication

One Step Hydrothermal Synthesis of Ni-MoS_2-RGO Bifunctional Electrocatalysts for HER and OER

Min Zhao[1,2], Gaoliang Zhou[1], Xiaoman Liu[1], Xinyi Shen[1], Jianguo Lv[1,2,], Changjuan Hu[1], Ying Wang[1], Wei Tan[1], Shengjie Sun[1], Yuxuan Ma[1], Congrong Wang[1], Jin Yang[1], Miao Zhang[2, 3,*], Gang He[3,*], Lei Yang[4]*

[1] School of Physics and Materials Engineering, Hefei Normal University, Hefei 230601, China
[2] Key Laboratory for Photoelectric Detection Science and Technology of Education Department of Anhui Province, Hefei Normal University, Hefei 230601, China
[3] School of Physics and Material Science, Anhui University, Hefei 230039, China
[4] Department of Chemistry and Materials Engineering, Hefei University, Hefei 230601, China
[*]E-mail: lvjg1@163.com, zhmiao@ahu.edu.cn, hegang@ahu.edu.cn

Received: 11 November 2020 / *Accepted:* 30 December 2020 / *Published:* 31 January 2021

Pure MoS_2 and Ni-MoS_2-RGO were prepared by a one-step hydrothermal approach. The result indicated that intensity of XRD diffraction peaks for MoS_2 increase slightly as with the increase of RGO content. Mesopores of the MoS_2, Ni-MoS_2/RGO-10 and Ni-MoS_2/RGO-15 are mainly distributed in the pore diameter rage of 2-50 nm. The addition of RGO increase the layer numbers of MoS_2 in Ni-MoS_2/RGO. Two Raman characteristic peaks at about 378 and 400 cm^{-1} according to A_{1g} and E^1_{2g} modes have been observed in the MoS_2 and Ni-MoS_2/RGO. The eletrocatalytic test results show that the Ni-MoS_2/RGO-5 has the lowest overpotentials of 349 mV at a current density of 10 mA cm^{-2} for OER and the Ni-MoS_2/RGO-10 has the lowest overpotentials of 398 mV at a current density of 10 mA cm^{-2} for HER. Moderate Ni doping and RGO composites can effectively improve the intrinsic conductivity, the hydrogen adsorption free energy for HER, as well as providing more active sites for HER and OER.

Keyword: Ni-MoS_2-RGO; Oxygen evolution reaction; electrocatalysts; Hydrothermal method

1. INTRODUCTION

With the increase of energy demand and deterioration of environmental problems, sustainable and clean energy, such as solar energy, hydrogen energy and wind energy have been developed by researchers [1-3]. Among them, hydrogen has been considered to be the most promising alternative to traditional fossil energy. Electrocatalytic water splitting is considered to be an economical and effective way to produce hydrogen. The overall water splitting is depended on the overpotential and

kinetic process of hydrogen evolution reaction (HER) and oxygen evolution reaction (OER)[4-6]. In order to improve energy efficiency of the whole water splitting process, enhancing catalytic activity and reducing the overpotential for the HER and OER have been made by researchers. Due to the complex reaction mechanism for HER between electrocatalyst and OH^-, studies of HER in alkaline media are relatively rare. In addition, the reaction kinetics of the counterpart electrode reaction for the OER is relatively slow during overall water splitting[7, 8].

In recent years, transition metal sulfides have been investigated extensively due to its excellent electrocatalytic performance. Among them, molybdenum disulfide (MoS_2) have been paid much attention because of its two-dimensional layered structure. It is well known that the active sites in MoS_2 electrocatalysts are located at the unsaturated S atoms and the exposed Mo atoms [9]. However, some disadvantages (such as poor conductivity and few activity sites) limit its application in the field of electrocatalysis. Therefore, MoS_2 with few-layers structure, which has large specific surface area, high conductivity and multiple active border sites, have been constructed and designed by transition metal doping and compositing with other low-dimensional materials (such as reduced graphene oxide (RGO) sheets, carbon nanotubes and mesoporous carbon etc.) in recent years[10-12]. Therefore, combining MoS_2 with the carbon matrix to form heterostructure is also an effective method to improve the electrochemical properties. In addition, some reports indicated that doping of Fe, Co and Ni in the MoS_2 could adjust the electronic structure of MoS_2 so as to increase its electrical conductivity and decreasing the hydrogen adsorption energy for HER. However, there are few reports on the improvement of OER performance by transition metal doping.

Herein, Ni-doped MoS_2-RGO composites with different RGO contents (Ni-MoS_2-RGO) have been successfully synthetized by means of an one-step hydrothermal technique. Microstructure were measured via X-ray diffractometer, Raman spectrometer and surface area and porosity analyzer. The electrochemical results show that the pure MoS_2 present poor HER activities and OER activities in the alkaline media. The HER and OER activities could been enhanced by Ni doping and RGO composites.

2. EXPERIMENTAL

2.1. Preparation of sample

In order to synthesize the Ni-MoS_2/RGO, 18 g of ammonium molybdate, 0.27 g of L-cysteine and 0.06 mmol of nickel nitrate were first dissolved in 20 mL of deionized (DI) water. In order to obtain a homogeneous dispersion, the mixed solution was treated ultrasonic for 30 minutes. Then the graphene oxide (5mg, 10mg and 15mg) have been added into the mixed solution, which was treated ultrasonic for another 30 minutes. The mixed solution was then transferred to a 50 mL Teflon-lined stainless steel autoclave and kept in an oven at 200 ^oC for 12 h. The autoclave has been cooled to room temperature as the reaction is finished. The final products were washed with DI water and absolute ethanol for several times and dried at 60 °C for 12 h. The pure MoS_2 was synthetized for comparison. The final products were named as MoS_2, Ni-MoS_2/RGO-5, Ni-MoS_2/RGO-10 and Ni-MoS_2/RGO-15, respectively.

2.2. Characterizations

Crystal structure of the samples were investigated by a powder X-ray diffractometer (TD-3500) usingCu Ka radiation (Cu Kα, λ=1.5406Å). Raman spectra of the samples were measured by a Raman spectroscopy (inVia-Reflex, Renishaw) using 532 nm laser excitation. Pore structure of the samples were measured at 77 K using a surface area and porosity analyzer (V-Sorb 4800).

2.3. Electrochemical measurements

Electrochemical tests of the samples were measured by means of electrochemical workstation(CHI 660E) with a standard three-electrode system. Ag/AgCl electrode, catalyst coated carbon paper and carbon cloth were used as the reference, working and counter electrodes, respectively. In order to prepare the working electrode, 10 mg electrocatalyst was dissolved in a mixed solution of isopropyl alcohol (400 μL) and Nafion (5.0 wt%, 25 μL), which was ultrasonically dispersed for 1h to form a homogeneous ink. Then, the ink was dropped onto a carbon paper of 1.0×1.0 cm^2. The working electrode was dried for 12 h at 60 °C in a vacuum oven. Linear scan voltammetry (LSV) was tested at a rate of 10 mV s^{-1} in a N_2-saturated 1 M KOH solution. The potentials vs. Ag/AgCl were converted to the reversible hydrogen electrode (RHE) using the following relationship [13]:

$$E_{RHE} = E_{Ag/AgCl} + 0.059\times pH + 0.1976\ V \quad (1)$$

where E_{RHE} is the potential vs. RHE and $E_{Ag/AgCl}$ is the potential *vs.* Ag/AgCl electrode. All potentials were *iR*-compensated. Electrochemical impedance spectroscopy (EIS) spectrum was measured in the frequency range of 10^5 to 0.01 Hz with an overpotential of 0.3 V and applied potential amplitude of 5 mV.

3. RESULTS AND DISCUSSION

Fig. 1 gives the XRD patterns of the samples. Two diffraction peaks centered at about 33.5° and 58.3° are corresponded to (101) and (110) planes can be observed in the pure MoS_2 material, which can be assigned to hexagonal phase MoS_2 (JCPDS No. 37-1492). No obvious diffraction peak from the (002) plane has been observed. The results may be attributed to the lower reaction temperature. When the content of RGO in the MoS_2 increases, the intensity of diffraction peaks for MoS_2 increases slightly. For the sample with 10 mg of graphene oxide, one obvious diffraction peak centered at about 17.7° from the *d* spacings of 4.75 Å may be assigned to the low crystallinity of MoS_2[14, 15].

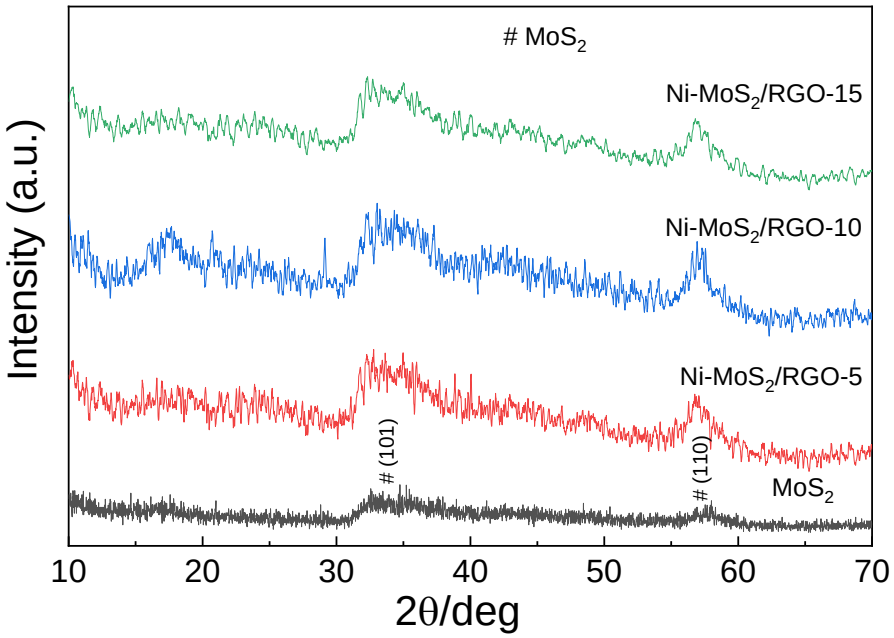

Figure 1. XRD patterns of MoS_2, Ni-MoS_2/RGO-5, Ni-MoS_2/RGO-10 and Ni-MoS_2/RGO-15, respectively.

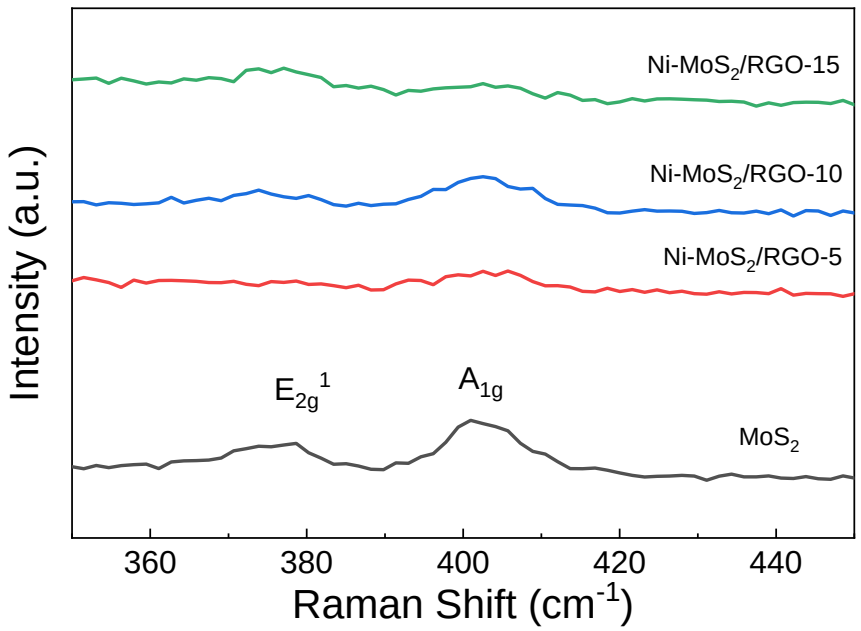

Figure 2. Raman spectra of MoS_2, Ni-MoS_2/RGO-5, Ni-MoS_2/RGO-10 and Ni-MoS_2/RGO-15, respectively.

Fig.2 presents the Raman spectra of the MoS_2, Ni-MoS_2/RGO-5, Ni-MoS_2/RGO-10 and Ni-MoS_2/RGO-15. Two Raman characteristic peaks from MoS_2 centered at about 378 and 400 cm^{-1} may be indexed to the E^1_{2g} in-plane vibration phonon mode of two S atoms with opposite orientation with respect to Mo atom and A_{1g} out-of-plane vibration phonon mode of S atoms, respectively [16, 17].

Similar Raman characteristic peaks also can be seen in the Ni-MoS_2/RGO samples. It is well known that the frequency differences (Δk) of A_{1g} and E^1_{2g} modes can be used to survey the layer number of MoS_2 [18]. It can be seen that in the Raman spectrum of Ni-MoS_2/RGO-10, the A_{1g} out-of-plane vibration phonon mode blue shifts to 403 cm^{-1} and the E^1_{2g} in-plane vibration phonon mode red shifts to 373 cm^{-1}. Compared with the Δk value of 22 cm^{-1} for pure MoS_2, the Ni-MoS_2/RGO-10 has the higher Δk value of 30 cm^{-1}. The results indicated that the addition of RGO increases the layer numbers of MoS_2 in Ni-MoS_2/RGO-10 [19].

Experiment of nitrogen desorption and adsorption was adopted to measure the pore structure of the samples. It can be seen from the Fig. 3a that all of the curves show type-IV isotherms with an evident hysteresis loop, indicating all the samples present mesoporous structures. Fig. 3b gives the BJH pore diameter distribution curves of the samples. The result indicates that mesopores of the MoS_2, Ni-MoS_2/RGO-10 and Ni-MoS_2/RGO-15 are mainly distributed in the pore diameter rage of 2-50 nm. However, the mesopores of the Ni-MoS_2/RGO-5 are mainly distributed in the pore diameter rage of 2-6 nm. Massive mesopores is beneficial to the exposure of catalytic active sites and rapid transport of HER and OER relevant species.

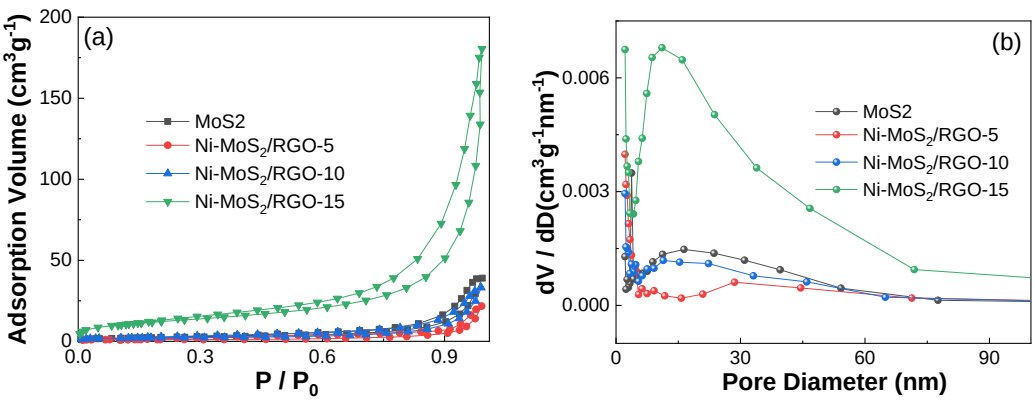

Figure 3. (a) N_2 adsorption-desorption isotherms and (b) pore size distribution curves of MoS_2, Ni-MoS_2/RGO-5, Ni-MoS_2/RGO-10 and Ni-MoS_2/RGO-15, respectively.

It is critically important to develop an electrocatalyst with bifunctional OER and HER catalytic activity for overall water splitting. In this letter, the OER activities of the samples were measured in 1 M KOH solution. Fig. 4a shows the LSV polarization curves of all the samples for OER. The overpotentials at a current density of 10 mA cm^{-2} are 423, 349, 351 and 350 mV for MoS_2, Ni-MoS_2/RGO-5, Ni-MoS_2/RGO-10 and Ni-MoS_2/RGO-15, respectively. Ni-MoS_2/RGO-5 shows great promotion than MoS_2 in the OER activity, which may be due to improvement of the OER active sites[20]. The results indicated that Ni-MoS_2/RGO-5 shows the lowest overpotentials, which is much less than the overpotentials of 540 mV for Co-MoS_2-0.5 in 0.5 M H_2SO_4 [10]. The catalytic activity and the OER reaction kinetics also can be presented by Tafel slope value, which can be calculated by LSV polarization curves for OER. As shown in Fig.4b, the Tafel slope values of MoS_2, Ni-

MoS_2/RGO-5, Ni-MoS_2/RGO-10 and Ni-MoS_2/RGO-15 are 373.4, 145.9, 139.7 and 122.1 mV dec^{-1}, respectively.

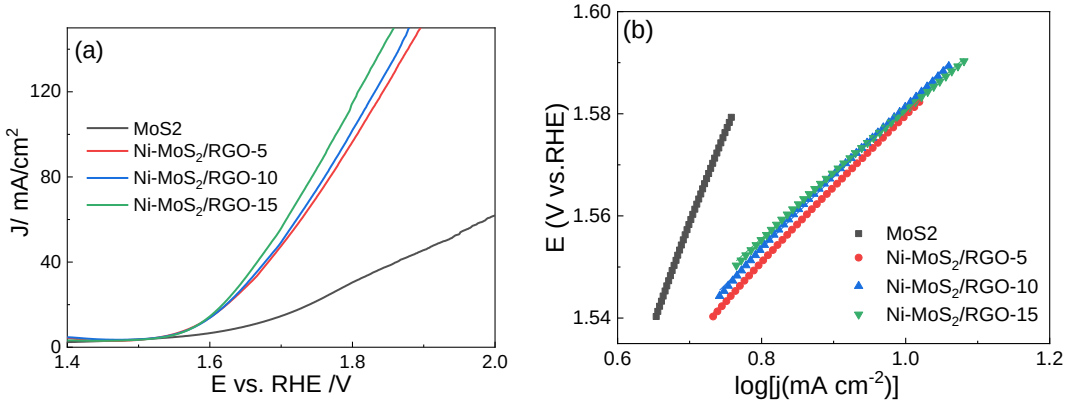

Figure 4. (a) OER polarization curves and (b) corresponding Tafel plots of MoS_2, Ni-MoS_2/RGO-5, Ni-MoS_2/RGO-10 and Ni-MoS_2/RGO-15.

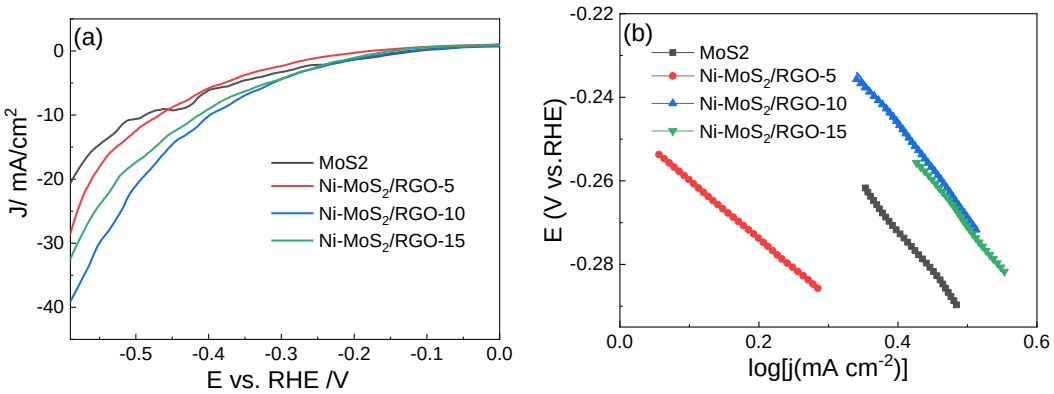

Figure 5. (a) HER polarization curves and (b) corresponding Tafel plots of MoS_2, Ni-MoS_2/RGO-5, Ni-MoS_2/RGO-10 and Ni-MoS_2/RGO-15.

In addition to the OER, eletrocatalytic HER activity of the samples were also investigated based on the LSV polarization curves (Fig. 5a) in 1M KOH solution. Similar to the OER activities of the samples, involving Ni doping and compound with RGO would improve significantly HER performance of the samples. In order to achieve 10mA cm^{-2} HER current density, MoS_2 needed high overpotential (485 mV). In compared to the MoS_2, Ni-MoS_2/RGO-5, Ni-MoS_2/RGO-10 and Ni-MoS_2/RGO-15 required lower overpotentials of 468, 398 and 413 mV, respectively. It can be seen that Ni-MoS_2/RGO-10 shows the lowest overpotentials, which is better than the previous results for MoS_2 materials (~0.460 V) [21]. The HER reaction kinetics also can be provided by Tafel slope value, which can be calculated by LSV polarization curves for HER. As shown in Fig.5b, the Tafel slope values of MoS_2, Ni-MoS_2/RGO-5, Ni-MoS_2/RGO-10 and Ni-MoS_2/RGO-15 are 203.0, 140.2, 214.0 and 214.1 mV dec^{-1}, respectively. The experimental results demonstrated that moderate Ni doping and RGO composites could effectively regulate electronic structure and eletrocatalytic active sites in the MoS_2,

and then improving the conductivity, decreasing the hydrogen adsorption free energy for HER, as well as increasing active sites for HER and OER[10].

4. CONCLUSIONS

In summary, bifunctional electrocatalysts Ni-MoS_2-RGO have been realized via a sample one-step hydrothermal approach. The content of RGO in the MoS_2 have little effect on the intensity of diffraction peaks of MoS_2. Δk value of Ni-MoS_2/RGO-10 is larger than that of pure MoS_2, indicating that the addition of RGO increases the layer numbers of MoS_2 in Ni-MoS_2/RGO-10. The Ni-MoS_2/RGO-5 has the lowest overpotentials of 349 mV at a current density of 10 mA cm^{-2} for OER and the Ni-MoS_2/RGO-10 has the lowest overpotentials of 398 mV at a current density of 10 mA cm^{-2} for HER. Electronic structure and eletrocatalytic active sites in the MoS_2 could be regulated by moderate Ni doping and RGO composites. The results provide a novel idea for the development of low cost and efficient electrocatalysts for overall water splitting.

ACKNOWLEDGEMENTS
This work was supported by National Natural Science Foundation of China (Nos. 51701001, 61804039, 51802145), Academic funding projects for Top Talents in Subjects (Majors) of Universities (No. gxbjZD31), Natural Science Foundation of Anhui Higher Education Institution of China (KJ2019A0734, KJ2017A924, KJ2017A002, KJ2019A0735), Natural Science Foundation of Anhui Province (No. 1808085QE126), Provincial quality engineering project of colleges and universities in Anhui Province (2020jxtd210) and Universities Joint Key Laboratory of Photoelectric Detection Science and Technology in Anhui Province(Grant No. 2020GDTCZD01).

References

1. J. Hu, J. Chen, H. Lin, R. Liu, X. Yang, *J. Solid State Chem.,* 259 (2018) 1.
2. Z. Xi, A. Mendoza-Garcia, H. Zhu, M. Chi, D. Su, D.P. Erdosy, J. Li, S. Sun, *Green Energy Environ.,* 2(2017) 119.
3. Y. Wang, Y. Pan, L. Zhu, H. Yu, B. Duan, R. Wang, Z. Zhang, S. Qiu, *Carbon*, 146 (2019) 671.
4. A. Li, K. Shen, J. Chen, Z. Li, Y. Li, *Chem. Eng. Sci.,* 166 (2017) 66.
5. W.H. Guo, Q. Zhang, X.H. Wang, Y.X. Yang, X.L. Li, L.J. Li, H.Q. Luo, N.B. Li, *Electrochim. Acta*, 357 (2020) 136850.
6. Q. Chen, X. Zhang, S. Li, J. Tan, C. Xu, Y. Huang, *Chem. Eng. J.,* 395 (2020) 125130.
7. H. Li, X. Qian, C. Xu, S. Huang, C. Zhu, X. Jiang, L. Shao, L. Hou, *ACS Appl. Mater. Interfaces,* 9 (2017) 28394.
8. R. Liu, H. Zhang, X. Zhang, T. Wu, H. Zhao, G. Wang, *Rsc Adv.*, 7 (2017) 19181.
9. C. Wang, *Int. J. Electrochem. Sci.,* 14(2019) 9805.
1. 10.Q Xiong, X Zhang, H Wang, G Liu, G Wang, H Zhang, H Zhao, *Chem. Commun.,* 54(2018)3859.
10. X. Guo, Y. Hou, R. Ren, J. Chen, *Nanoscale Res. Lett.,* 12 (2017) *479*.
11. S. Zhang, B.V.R. Chowdari, Z. Wen, J. Jin, J. Yang, *Acs Nano,* 9 (2015) 12464.
12. Z. Cao, M. Wu, H. Hu, G. Liang, C. Zhi, *NPG Asia Mater.,* 10 (2018) 670.
13. L. Chen, W. Yang, X. Liu, J. Jia, *Int. J. Hydrogen Energy*, 42 (2017) 12246.

14. J. Xie, J. Zhang, S. Li, F. Grote, X. Zhang, H. Zhang, R. Wang, Y. Lei, B. Pan, Y. Xie, *J. Am. Chem. Soc.*, 135 (2013) 17881.
15. Z. Pan, Z. Xia, Y. Tao, X. Shen, *Catal. Commun.*, 125 (2019) 56.
16. W. Jian, X. Cheng, Y. Huang, Y. You, R. Zhou, T. Sun, J. Xu, *Chem. Eng. J.*, 328 (2017) 474.
17. D. Qi, S. Li, Y. Chen, J. Huang, *J. Alloys Compd.*, 728 (2017) 506.
18. W.K. Jo, J.Y. Lee, N.C.S. Selvam, *Chem. Eng. J.*, 289 (2016) 306.
19. X. Yang, X. Wu, Z. Guo, Q. Li, H. Wang, C. Ke, W. Zeng, X. Qiu, Y. He, X. Liang, Y. Kim, *RSC Adv.*, 10 (2020) 33327.
20. S. Li, S. Wang, M.M. Salamone, A.W. Robertson, S. Nayak, H. Kim, S.C.E. Tsang, M. Pasta, J.H. Warner, *ACS Catal.* 7 (2017) 877.